Large Eddy Simulation: A Modellers Perspective

Michael Fitzmaurice, Yaping Shao
CANCES
The University of New South Wales
Sydney, Australia

The Large Eddy Simulation (LES) approach simulates a turbulent flow by solving the large scales of motion while modeling the small scales (subgrid), typically with an eddy viscosity closure. This paper presents a Modellers perspective of what are the 2 most important elements of the LES model, (1) making the LES Reynolds number R_{LES} large, and (2) preventing non-physical phenomena.

1 INTRODUCTION

Reynolds Averaging (RA) and Large Eddy Simulation (LES) are two common methods of simulating turbulent flow. The RA approach is to derive equations from the Navier Stakes equations, whose solution is the ensemble average of the turbulent flow being modeled. The derived equations contain terms that involve all scales of turbulent motion. To close this system of equations these terms must be modeled, either with eddy viscosity models or Reynolds Stress transport equations. The LES approach is to explicitly solve all the large scales of turbulent motion and model only the small scales (subgrid). Turbulent motion which is not resolved by the grid, constitutes the subgrid.

The first LES model was developed by (Deardorff, 1970) which was a 3 dimensional simulation of a turbulent channel flow. It contained 6720 nodes and used the Smagorinsky model (Smagorinsky et al., 1965) for the subgrid paramaterisation. Recent advancements of the LES technique include the use of more complex subgrid paramaterisations (Lesieur and Metais, 1996) (Germano et al., 1991), and the use of more nodes (500 thousand node simulations are now common).

In nature, turbulence occurs when the Reynolds number (R_e) is large. R_e is the ratio of inertial force to diffusion force. In natural flow, the only source of diffusion is molecular viscosity (ν), which results from molecular interactions in the fluid. Large eddy simulations contain additional sources of diffusion, numerical diffusion (ν_N) and turbulent diffusion (ν_T). The LES methodology requires the large scales of turbulent flow to be resolved explicitly, which necessitates the simulated flow to be turbulent. A LES Reynolds number is defined $R_{LES} = \frac{uL}{\nu+\nu_T+\nu_N}$, to determine if the simulated flow is turbulent. Consistent with natural flows, if R_{LES} is in the turbulent regime, the flow is turbulent.

Numerical diffusion results when the continuous Navier Stokes equations are discritised into a finite set of discrete equations. Numerical diffusion is large when upwind schemes are used for the discretisation of the advection term, and small when central schemes are used.

Turbulent diffusion results from the use of eddy viscosity models to paramaterise the subgrid. Eddy viscosity models are based on the Boussinesq assumption, which in the LES context, implies; the effect of the subgrid on the large scales, is qualitatively the same as molecular viscosity. The magnitude of the turbulent diffusion depends on the subgrid model, but is generally a function of the resolved flow field and the grid size.

Diffusion is a smoothing operator, which reduces gradients and amplitudes. It's presence in the LES equations encourages solutions which are smoother, and thus easier to represent with a finite number of discrete equations. Conversely, LES models with small diffusion will be difficult to represent with a finite set of discrete equations, and their solutions are susceptible to errors, which can manifest as non-physical phenomena.

If R_{LES} is large, turbulent solutions to the LES equations will exist. To initiate these solutions the inflow boundary conditions must be correctly specified. Two common methods are (1) use of periodic boundary conditions (Yang and Ferziger, 1993), (2) use results of a previous simulation. Periodic boundary conditions are popular because of their simplicity, but for many flow situations they may not be valid. For these situations method (2) may be necessary.

2 GOVERNING EQUATIONS

Flow is governed by the instantaneous momentum and continuity equations. The flux form of these equations in tensor notation, assuming summation over repeated indices, are (1)-(2) .

$$\frac{\partial u_i}{\partial t} + \frac{\partial u_i u_j}{\partial x_j} = \frac{\partial}{\partial x_j}(\nu \frac{\partial u_i}{\partial x_j}) - \frac{1}{\rho}\frac{\partial p}{\partial x_i} + S_i \quad (1)$$

$$\frac{\partial u_i}{\partial x_i} = 0 \tag{2}$$

u_i is the velocity tensor, t time, ν kinematic molecular viscosity, ρ density, p pressure, S_i momentum sink or source.

3 FILTERING

Prior to converting the continuous governing equation into discrete form they are filtered (3) with a low pass filter g, to isolate the subgrid effects.

$$\overline{u} = \int (g * u) dV \tag{3}$$

The filtered Navier Stokes equations become (4)-(5),

$$\begin{aligned} \frac{\partial \overline{u_i}}{\partial t} + \frac{\partial \overline{u}_i \overline{u}_j}{\partial x_j} &= \frac{\partial}{\partial x_j}(\nu \frac{\partial \overline{u_i}}{\partial x_j}) \\ &- \frac{1}{\rho}\frac{\partial \overline{p}}{\partial x_i} + \frac{\partial}{\partial x_j}(\overline{u}_i \overline{u}_j - \overline{u_i u_j}) \end{aligned} \tag{4}$$

$$\frac{\partial \overline{u_i}}{\partial x_j} = 0 \tag{5}$$

The $\frac{\partial}{dx_j}(\overline{u}_i \overline{u}_j - \overline{u_i u_j})$ term contains subgrid effects which need to be modeled.

4 MODEL

4.1 Discretisation

The Navier Stokes equations written in conservation form, for a generic variable ϕ are,

$$\frac{\partial \phi}{\partial t} + \nabla \cdot \mathbf{f} = S_\phi \tag{6}$$

The flux $\mathbf{f}$ is composed of advective $\mathbf{f^c} = \mathbf{u}\phi$ and diffusive $\mathbf{f}^d = -\Gamma_\phi \nabla \phi$ components. Integrating over a finite volume, and applying the divergence theorem to the flux term, (6) becomes (7).

$$\begin{aligned} \frac{\partial \phi}{\partial t}\Delta x \Delta y \Delta z &+ (f_e - f_w)\Delta y \Delta z \\ &+ (f_n - f_s)\Delta x \Delta z \\ &+ (f_t - f_b)\Delta x \Delta y \\ &= S_\phi \Delta x \Delta y \Delta z \end{aligned} \tag{7}$$

$f_e, f_w, f_n, f_s, f_t, f_b$ are the (advection-diffusion) fluxes in directions east, west north, south, top and bottom respectively. The time-dependent term, advection flux, diffusion flux and source term are each discritised separately.

4.1.1 Advection

The advection term is discritised with three schemes, $1st$ order upwind, $4th$ order central, and $5th$ order upwind. Consider the discretisation of flux f_e.

$$f_e = u_e \phi_{i+1/2,j} \tag{8}$$

$1st$ order upwind.

$$\phi_e = \begin{cases} \phi_{i,j} & \text{if } u_e \geq 0 \\ \phi_{i+1,j} & \text{if } u_e < 0 \end{cases} \tag{9}$$

$4th$ order central.

$$\phi_e = \frac{1}{16}(-1\phi_{i-1,j} + 9\phi_{i,j} + 9\phi_{i+1,j} - 1\phi_{i+2,j}) \tag{10}$$

$5th$ order upwind.

$$\phi_e = \begin{cases} \frac{1}{128}(3\phi_{i-2,j} - 20\phi_{i-1,j} + 90\phi_{i,j} \\ +60\phi_{i+1,j} - 5\phi_{i+2,j}) & \text{if } u_e \geq 0 \\ \frac{1}{128}(-5\phi_{i-1,j} + 60\phi_{i,j} \\ +90\phi_{i+1,j} - 20\phi_{i+2,j} + 3\phi_{i+3,j}) & \text{if } u_e < 0 \end{cases} \tag{11}$$

4.1.2 Diffusion

The diffusive flux is approximated by a $2nd$ order central scheme.

$$f^d_{i+1/2} = -\nu_\phi \frac{(\phi_{i+1} - \phi_i)}{x_{i+1} - x_i} + O(\Delta x)^2 \tag{12}$$

4.1.3 Time Dependent Term

Integration of (6) is performed fully implicitly in time. The time-dependent terms discretisation is $2nd$ order accurate involving 3 time levels.

$$\left(\frac{\partial \phi}{\partial t}\right)^n_{i,j,k} = \frac{3\phi^n_{i,j,k} - 4\phi^{n-1}_{i,j,k} + \phi^{n-2}_{i,j,k}}{\Delta t} + O(\Delta t)^2 \tag{13}$$

4.1.4 Pressure Term

The pressure gradients are approximated by central difference ($2nd$ order accurate in space).

$$\left(\frac{\partial p}{\partial x_i}\right)_{i+1/2,j,k} = \frac{p_{i+1,j,k} - p_{i,j,k}}{\Delta x} + O(\Delta x)^2 \quad (14)$$

4.2 Subgrid Model

The diffusive effect of the unresolved subgrid (turbulent diffusion) is assumed constant and set a value of 0.004. This differs with most subgrid models, which produce turbulent diffusions that are transient, spatially variant and a function of grid size (eg. Smagorinsky eddy viscosity closure (16)).

$$\overline{u_i}\overline{u_j} - \overline{u_i u_j} = 2\nu_T \overline{S}_{ij} \quad (15)$$

$$\nu_T = (C_s l)^2 \sqrt{2\overline{S}_{ij}\overline{S}_{ij}} \quad (16)$$

$$\overline{S}_{ij} = \frac{1}{2}\left(\frac{\partial \overline{u}_i}{\partial \overline{x}_j} + \frac{\partial \overline{u}_j}{\partial \overline{x}_i}\right) \quad (17)$$

$\overline{S}_{ij}$ is the resolved strain in the fluid, C_s Smagorinsky constant and l is representative of the grid size.

4.3 Equation Coupling

The continuity and momentum equations are coupled by projecting the velocity field produced by the momentum equations (u^*) into divergence free space (u^n) (ie. enforce continuity)(Patankar, 1980).

4.4 Solver

Solving the implicit set of discritised equations is performed by 2 solvers, the Thomas Algorithm line solver and Additive Corrective Multigrid.

4.4.1 Line Solver

The implicit set of equations for each node, can be written in tridiagonal form (18).

$$a\phi^n_{i-1,j,k} + b\phi^n_{i,j,k} + c\phi^n_{i+1,j,k} = d_i \quad (18)$$

Assembling all equations ror nodes of line $i = 1...n$ produces a tridiagonal matrix (19).

$$\begin{bmatrix} b_0 & c_0 & 0 & 0 & \dots & 0 \\ a_1 & b_1 & c_1 & 0 & \dots & 0 \\ 0 & a_2 & b_2 & c_2 & \dots & 0 \\ \vdots & \vdots & \vdots & \vdots & \ddots & \vdots \end{bmatrix} \begin{pmatrix} \phi_0 \\ \phi_1 \\ \phi_2 \\ \vdots \end{pmatrix} \begin{pmatrix} d_0 \\ d_1 \\ d_2 \\ \vdots \end{pmatrix} \quad (19)$$

Tridiagonal matrices are solved by the Thomas algorithm. The 4 steps to evaluate nodal values $\phi_0 \dots \phi_n$ are shown in (20) to (24).

$$c'_0 = \frac{c_0}{b_0} \quad d'_0 = \frac{d_0}{b_0} \quad (20)$$

$$\text{for} \quad i = 1 \dots n \quad c'_i = \frac{c_i}{b_i - a_i c'_{i-1}} \quad (21)$$

$$d'_i = \frac{d_i - a_i d'_{i-1}}{b_i - a_i c'_{i-1}} \quad (22)$$

$$\phi_n = d'_n \quad (23)$$

$$\text{for} \quad i = n-1 \dots 0 \quad \phi_i = d'_i - \phi_{i+1} c'_i \quad (24)$$

Accurate solutions from the Thomas Algorithm require the tridiagonal matrix to be well conditioned (25).

$$|b_i| > |a_i| + |c_i| \quad (25)$$

4.4.2 Additive Corrective Multigrid

The Additive Corrective Multigrid (ACM) (Hutchinson and Raithby, 1986), involves decomposing the fine grid ($64 \times 32 \times 32$) into 3 coarse grids ($32 \times 16 \times 16$), ($16 \times 8 \times 8$) and ($8 \times 4 \times 4$). The ACM equations are derived from the coefficients of the fine grid equations. The coarse grid equations are solved by Thomas algorithm, and the fine grid solution is then corrected.

4.5 Boundary Conditions

4.5.1 Lower and Upper boundary

Dirichlet no-slip boundary conditions are applied at the lower boundary ($u = v = w = 0$). Neumann and Dirichlet boundary conditions are applied at the upper boundary ($\frac{\partial u}{\partial y} = \frac{\partial w}{\partial y} = 0 = v$).

4.5.2 Streamline and Cross-stream boundary

Periodic boundary conditions are applied in the stream-line and cross-stream directions ($\phi_0 = \phi_n$ and $\phi_{n+1} = \phi_1$). This results in a matrix which contains coefficients in the upper right and lower left, and are solved in accordance with (Strikwerda, 1990)

4.6 Solution Procedure

The coupled momentum and continuity equations are solved by the SIMPLE method (Patankar, 1980).

5 TEST CASE

The Large Eddy Simulation model described in Section 4 is applied to solve the flow at a 20% porous windbreak (see Figure 3). The domain size is $72 \times 16 \times 16m^3$, and is discritised on a staggered $64 \times 32 \times 32$ uniformly spaced structured grid. The porous windbreak extends across the entire width of the domain and is $4m$ (8 nodes) high, and is modeled with a linear momentum sink in the streamline momentum equation.

$$S_x = \rho\delta(x)k|u|u \tag{26}$$

$$\int_{-\infty}^{\infty} \delta(x)dx = 1 \tag{27}$$

$$k = 8.0 \tag{28}$$

Flow is maintained by the application of a constant pressure gradient in the x direction.

$$S_x = \frac{P_L - P_0}{L} \tag{29}$$

6 RESULTS

6.1 Advection Scheme

To model a turbulent flow with LES, the R_{LES} of the simulation must be large (in the turbulent regime). This requires the molecular diffusion, numerical diffusion, and turbulent diffusion to be small. Molecular diffusion is always small. Turbulent diffusion can be made small by using less diffusive models or reducing grid size. The magnitude of the numerical diffusion is dependent on the scheme used to discritised the advection term.

The $4th$ order central scheme has negligible numerical diffusion and as a consequence R_{LES} is large and a turbulent flow was produced. Unfortunately, the central scheme is prone to produce non-physical oscillations, which occurred in front of the windbreak, as illustrated in Figure 4. It is pertinent to mention that the presence of oscillations or other non-physical characteristics are difficult to observe in turbulent flow simulations. The oscillations only became evident when an ensemble average of the flow was made.

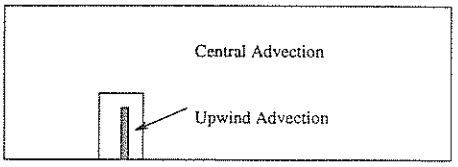

Figure 1: Advection Domains

The oscillations are confined to regions of large gradients, particularly when the flow is decelerating. To prevent oscillations, $1st$ order and $5th$ order upwind advection schemes were tried. The $1st$ order upwind schemes successfully prevents oscillations, but proved too numerically diffusive, R_{LES} was in the laminar regime, and a turbulent flow could not be achieved. The $5th$ order upwind scheme was not able to prevent the development of oscillations.

To prevent the oscillations, while maintaining a R_{LES} in the turbulent regime, the computational domain was decomposed into 2 regions (see Figure 1), with a $1st$ order upwind scheme used in the vicinity of the windbreak and a central scheme used elsewhere. This is numerically the same as modeling the windbreak with a momentum sink and a momentum diffuser (30).

$$S = \rho\delta(x)k|u|u + \frac{\partial}{\partial x_j}(\nu_N \frac{\partial \overline{u_i}}{\partial x_j}) \tag{30}$$

$$\nu_N = \text{numerical diffusion produced by upwind scheme} \tag{31}$$

This approach was successful in preventing the oscillations, while the large R_{LES} outside the windbreak region permitted the development of turbulence.

An indication of the effect of diffusion on a turbulent flow field can be assessed from Figure 5. The streamwise velocity variance σ_u^2 (turbulence intensity) is expected to be large near the top of the windbreak, however it is very small in this region. Obviously the turbulent intensity is dissipated by the large numerical diffusion in the windbreak region.

6.2 Boundary Conditions

The most convenient inflow boundary conditions for LES are periodic. However, if the flow is not periodic, the domain must be chosen sufficiently long to negate the influence of obstacles in the flow.

Numerical results (Wang and Tackle, 1995) and experimental data (Wilson, 1985), suggests flow past a windbreak fully recovers 18 windbreak heights (h) downstream from the break. Streamlines of the simulated flow is illustrated in Figure 6. The streamlines

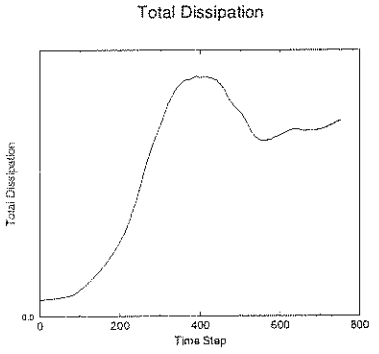

Figure 2: Total Dissipation

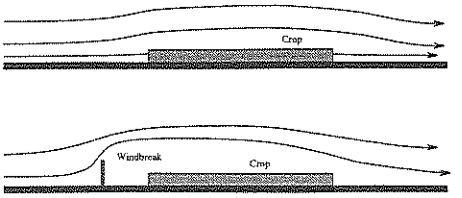

Figure 3: Windbreak

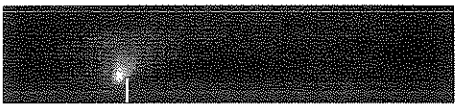

Figure 4: non-Physical Oscillations

are horizontal at the inflow, they are disrupted by the break, separation, re-attachment and circulation occurs before the streamlines re-establishes horizontal trajectories. Similar information can be deseminated from Figure 8. They support (Wang and Tackle, 1995) and (Wilson, 1985) contention that flow recovers within $18h$[1].

Figure 5 illustrates the variance of streamwise velocity, which clearly indicates that the effect of the windbreak is propagated downstream further than $18h$. This suggests that an analysis of the persistence of both the mean and higher moments may be necessary before the domain sizes of a periodic boundary is chosen.

6.3 Generating Turbulence and determing if it is Statistically Steady

A 20% porous windbreak sufficiently disrupted the flow field to allow the initially laminar flow to become turbulent. No additional turbulence generation mechanisms were necessary, such as peturbing the flow field with random fluctuations.

An indication of the time of turbulent transition and the establishment of statistically steady turbulence can be ascertained from a time series plot of the dissipation function (32). This is a component of the energy equation for flow, and it measures the amount of energy an elemental volume dissipates to viscous stresses.

Figure 2 is a plot of the dissipation function, integrated over all control volumes of the domain, for each time step. The total dissipation increases as the flow becomes turbulent, before reaching a peak, and then becoming level. It has been determined that the level section of the curve corresponds to a statistically steady turbulent flow.

[1]domain is $18h$ long

$$\phi = 2\nu(S_{ij}S_{ij}) \tag{32}$$

ϕ is the dissipation function and ν the total viscosity (numerical+molecular+turbulent).

6.4 Solver

Two solvers were tried, the Thomas Algorithm line solver and the Additive Corrective multigrid. The line solver converged the momentum equations rapidly, but the pressure correction equation converged very slowly. The multigrid solver did not affect the rate of convergence of the momentum equations, but the convergence rate of the pressure correction equation was increased by a factor of 10 on a $64 \times 32 \times 32$ grid.

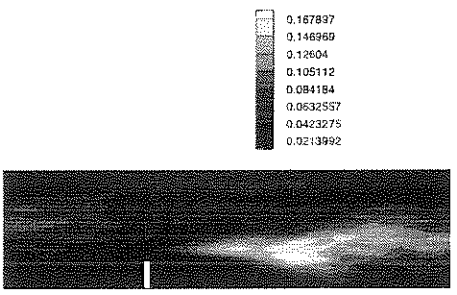

Figure 5: σ_u^2

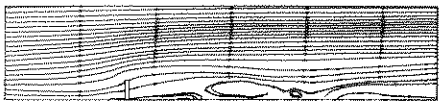

Figure 6: Average Stream Lines

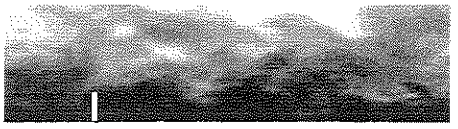

Figure 7: Instantaneous U velocity

7 CONCLUSIONS

1. R_{LES} must be large (in the turbulent regime) for LES to simulate turbulent flow. This necessitates the use of non-diffusive advection schemes to minimize numerical diffusion, and fine grids, so the diffusion produced by the subgrid model is small.

2. In regions of large gradients, grid refinement or diffusive advection schemes must be used to prevent oscillations, or other non physical effects.

3. A 20% porous windbreak sufficiently perturbed the flow to generate turbulence.

4. The amount of energy in the LES flow dissipated to shear, indicates the time of turbulent transition and when statistically steady turbulence is achieved.

5. Line solvers are adequate for the momentum equations. The convergence rate of the pressure correction equation is accelerated by a factor of 10 if Additive Corrective Multigrid is used, for a $64 \times 32 \times 32$ grid..

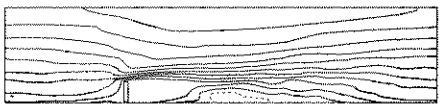

Figure 8: Average Streamline Velocity

References

Deardorff, J. (1970). A numerical study of three-dimensional turbulent channel flow at large reynolds numbers. *Physics Fluids A*, 41(2):453–480.

Germano, M., Piomelli, U., Moin, P., and Cabot, W. (1991). New trends in large-eddy simulations of turbulence. *Physics Fluids A*, 3(7):1760–1765.

Hutchinson, B. and Raithby, G. (1986). A multigrid method based on the additive correction strategy. *Numerical Heat Transfer*, 9:511–537.

Lesieur, M. and Metais, O. (1996). New trends in large-eddy simulations of turbulence. *Annual Review Fluid Mechanics*, 28:45–82.

Patankar, S. (1980). *Numerical Heat Transfer*. Hemisphere.

Smagorinsky, J., Manabe, S., and Holloway, J. (1965). *Mon. Weath. Rev.*, 93:727.

Strikwerda, J. (1990). *Finite Difference Schemes and Partial Differential Equations*. Wadsworth and Brooks.

Wang, H. and Tackle, E. (1995). A numerical simulation of boundary-layer flows near shelterbelts. *Boundary Layer Meteorology*, 75:141–173.

Wilson, J. (1985). Numerical studies of flow through a windbreak. *J. Wind Engineering Industrial Aerodynamics.*, 21:119–154.

Yang, K. and Ferziger, J. (1993). Large-eddy simulation of turbulent flow in a channel with a surface mounted two dimensional obstable using a dynamic subgrid scale model. *AIAA*, 93(0542).